RSC Advances

PAPER

View Article Online
View Journal | View Issue

Cite this: *RSC Adv.*, 2020, **10**, 33851

Synthesis and characterization of a hyaluronic acid-based hydrogel with antioxidative and thermosensitive properties†

Meng Chen,‡[a] Cui Li,‡[a] Fujiao Nie,[a] Xiaoyan Liu,[a] Iraklis I. Pipinos[b] and Xiaowei Li*[a]

Peripheral arterial disease (PAD) is initiated by progressive atherosclerotic blockages of the arteries supplying the lower extremities. The most common presentation of PAD is claudication (leg pain and severe walking limitation), with many patients progressing to limb threatening ischemia and amputation. Biomaterial approaches are just beginning to be explored in the therapy of PAD with different materials now being evaluated for the delivery of cells or growth factors in animal models of PAD. A biomaterial matrix optimized for minimally invasive injection in the ischemic leg muscles of patients with PAD is urgently needed. There are several important requirements for optimal delivery, retention, and performance of a biomaterial matrix in the mechanically, histologically, and biochemically dynamic intramuscular environment of the PAD leg. Ideally, the material should have mechanical properties matching those of the recipient muscle, undergo minimal swelling, and should introduce properties that can ameliorate the mechanisms operating in PAD like oxidative stress and damage. Here we have developed an injectable, antioxidative, and thermosensitive hydrogel system based on hyaluronic acid (HA). We first synthesized a unique crosslinker of disulfide-modified poloxamer F127 diacrylate. This crosslinker led to the creation of a thermosensitive HA hydrogel with minimal swelling and muscle-matching mechanical properties. We introduced unique disulfide groups into hydrogels which functioned as an effective reactive oxygen species scavenger, exhibited hydrogen peroxide (H_2O_2)-responsive degradation, and protected cells against H_2O_2-induced damage. Our antioxidative thermosensitive HA hydrogel system holds great potential for the treatment of the ischemic legs of patients with PAD.

Received 2nd June 2020
Accepted 4th September 2020

DOI: 10.1039/d0ra07208g

rsc.li/rsc-advances

1 Introduction

Peripheral arterial disease (PAD) affects over 200 million adults worldwide and 8–10 million people in the US.[1,2] PAD is a manifestation of atherosclerosis that produces progressive narrowing and occlusion of the arteries supplying the lower extremities. The most common clinical manifestation of PAD is claudication (leg pain and severe walking limitation), but many patients progress to limb threatening ischemia and amputation.[1–3] Standard therapies for claudication include medication, supervised exercise therapy, and operative endovascular and open revascularization.[1–3] Unfortunately, all of them have significant limitations: modest efficiency for pharmacotherapy, poor compliance and limited utilization for exercise therapy, and considerable morbidity and poor long-term patency for revascularization.[1,2] Several types of clinical trials have been ongoing for newer PAD treatments, including cell/stem cell, gene, and growth factor therapies but have not yet translated to clinical benefit.[4–7] In particular the newer and most promising yet therapy using stem cells is plagued by poor retention and survival of these transplanted cells.[8,9]

Tissue engineering approaches are just beginning to be investigated as treatment modalities in PAD.[9–13] A biomaterial matrix could act as a standalone treatment with several potential advantages including off-the-shelf availability, reduced cost, and the ability to locally stimulate and support endogenous cells for tissue repair.[10–13] A number of different biomaterials have been evaluated for delivery of cells or growth factors in the ischemic limbs of animal models of PAD. For example, Rao *et al.* have developed and tested a decellularized skeletal muscle extracellular matrix (ECM) as a revascularization treatment in a mouse model of hindlimb ischemia by using the matrix to promote the delivery of cells, including myoblasts and fibroblasts.[13] However, the creation of ECM that has well-defined composition and complete removal of all cellular components is still difficult to achieve.[14,15] More recently Anderson *et al.* have

[a]*Mary & Dick Holland Regenerative Medicine Program, Department of Neurological Sciences, University of Nebraska Medical Center, Omaha, NE 68198, USA*

[b]*Department of Surgery, University of Nebraska Medical Center, Omaha, NE 68198, USA*

† Electronic supplementary information (ESI) available. See DOI: 10.1039/d0ra07208g

‡ These authors contributed equally to this work.

applied alginate hydrogels to locally deliver growth factors to enhance perfusion in the ischemic limb of a rabbit model.[16] The alginate hydrogels are produced by physical ionic-crosslinking which makes them brittle and may hamper their retention in the dynamic intramuscular environment. These limitations point to an urgent need for a biomaterial matrix that will be optimized for minimally invasive delivery in skeletal muscles that are compromised by PAD and other diseases.

There are several key requirements for optimal retention and delivery of a biomaterial in the intramuscular environment of the lower limb. First, the mechanically dynamic intramuscular environment may require a material that (a) undergoes minimal swelling once inside the target tissue and (b) has mechanical properties matching those of the recipient muscle [shear storage modulus (G'): ~2 kPa (rat) and ~7 kPa (swine)] while allows cell infiltration for integration.[8,17–20] The current approaches for the production of hydrogels have not fully addressed these key requirements especially for skeletal muscle applications. Specifically, interpenetrating double network hydrogels make injection unfeasible;[17] orthogonally crosslinking hydrogels have high swelling ratio;[18] purely ionically-crosslinked systems undergo significant plastic deformation making them fragile;[19] and clay nanocomposite hydrogels are too stiff for the intramuscular environment.[20] Second, rapid *in situ* formation is desirable to facilitate delivery using small gauge needles that will allow for injection of the material while it is still in liquid form with conversion into a hydrogel once in the target tissue. Finally, a myopathy is present in the legs of patients with PAD[21,22] and oxidative stress/damage is one of the main mechanisms operating to produce this well described muscle damage.[23–25] Therefore adding antioxidant properties to the hydrogel may introduce additional advantages to the management of the ischemic myopathy of PAD.[26]

Our group has previously applied an *in situ* crosslinkable hydrogel system based on hyaluronic acid (HA) for brain and soft tissue regeneration.[27–30] In a rat model for traumatic brain injury by controlled cortical impact, this HA hydrogel promoted significant vasculature network formation filling the lesion site. Most importantly, this HA hydrogel with G' of less than 0.1 kPa is porous enough to allow robust cell infiltration and migration.[28,31,32] Changing our focus from the brain and trauma to the skeletal muscle in PAD we aimed to modify the properties of this HA hydrogel by increasing its stiffness to match that of skeletal muscle, by reducing its propensity to swell, by modifying it with thermo-sensitivity to allow for injecting while liquid with rapid change into a final solid form in the target tissue, and by introducing elements with antioxidative properties. We have thus synthesized a unique macromer: disulfide-modified poloxamer F127 diacrylate (F127-SS-DA)[33–35] and we have explored the stiffness, swelling, temperature-sensitivity of HA hydrogels crosslinked by F127-SS-DA. Disulfides have antioxidant properties because they can participate in oxidative reactions as scavengers responding to hydrogen peroxide (H_2O_2) and superoxide.[36,37] Accordingly, we have also investigated the antioxidant and cell-protective characteristics of our new HA hydrogel in conditions involving H_2O_2-induced oxidative damage.

2 Materials and methods

2.1 Materials

All chemicals were used as received unless otherwise described. Thiolated hyaluronic acid (HA-SH) was purchased from Advanced BioMatrix, Inc. (Carlsbad, CA). Triethylamine (TEA), acryloyl chloride, 3-buten-1-ol, 1-ethyl-3-[3-(dimethylamino) propyl] carbodiimide (EDC), 3,3′-dithiobis(propanoic acid) (DTP), *N*,*N*-dimethylaminopyridine (DMAP), *t*-butyl methyl ether, 2,2-diphenyl-1-picrylhydrazyl (DPPH), and Pluronic F127 (MW 12.6 kDa) were obtained from Aldrich Chemical Co. (Milwaukee, WI). Dichloromethane (DCM) was purchased from Alfa Aesar (Ward Hill, MA). All other chemical reagents were obtained from Sigma-Aldrich (St. Louis, MO).

2.2 Synthesis of F127-DA and F127-SS-DA

2.2.1 F127-DA synthesis. First, F127 was dissolved in 40 mL DCM. TEA was added into the stirred F127 solution. After 5 min, acryloylchloride was added slowly *via* syringe. The mixture was stirred at ambient temperature for 72 h. Second, the mixture was concentrated under reduced pressure to a volume of 20 mL and then filtered to remove precipitated triethylamine hydrochloride. The solution was poured into 300 mL *t*-butyl methyl ether to precipitate the diacrylate product. The product was then collected by filtration. Finally, the product was dissolved in 50 mL water, dialyzed for 7 days, and lyophilized to obtain F127-DA. The structures of F127 and F127-DA were inspected by the Bruker Avance-III HD 500 MHz NMR spectrometer (Billerica, MA).

2.2.2 F127-SS-DA synthesis. F127 was dissolved in 40 mL DCM followed by the addition of EDC and DMAP. After 5 min, DTP was added. The mixed solution was stirred for 24 h at room temperature. The mixture was concentrated under reduced pressure to a volume of 20 mL, poured into 200 mL *t*-butyl methyl ether to precipitate the product, which was further collected by filtration. The product was then dissolved in 50 mL water, dialyzed for 7 days, and lyophilized to obtain the intermediate SS-F127-SS.

SS-F127-SS was dissolved in 15 mL DCM followed by the addition of EDC and DMAP. After 5 min, 3-buten-1-ol was added and stirred for 24 h at room temperature. The mixture was then poured into 200 mL *t*-butyl methyl ether to precipitate the product, which was collected by filtration. The solid was then dissolved in 50 mL water, dialyzed for 7 days, and lyophilized to obtain the final product F127-SS-DA. The structures of SS-F127-SS and F127-SS-DA were confirmed by the Bruker Avance-III HD 500 MHz NMR spectrometer.

2.3 Rheological characterization of HA hydrogels

To prepare HA hydrogels, various amounts of F127-SS-DA or F127-DA (10, 20, and 50 mg mL^{-1}) were mixed with HA-SH solution (4 mg mL^{-1}) and then kept at 4 °C overnight. Rheometer (HR-2, TA Instruments) was used to measure mechanical properties of these hydrogels, such as shear storage modulus (G'), shear loss modulus (G''), and gelation temperature. The rheological characterization of hydrogels was

performed by oscillation strain (1–10% strain; 1 Hz) and temperature (4–37 °C; 1 Hz, and 1% strain) sweeps as we reported previously.[29]

2.4 Radical scavenging activity

We have adopted a DPPH assay to examine scavenging activity of these synthesized polymers as reported previously.[36] Briefly, DPPH was dissolved in methanol to make a stocking solution (50 μM). DPPH solution (50 μL) was then mixed with 50 μL of a series of polymer solutions (F127-DA or F127-SS-DA: 0, 1.6, 3.1, 6.3, 12.5, 25, 50, 100 mg mL^{-1}). Ascorbic acid (AA, 50 mM) was used as a positive control. All samples were kept in the dark on a shaker at 200 rpm for 30 min. Absorbance values were measured at 517 nm using a Biotek Synergy H1 Hybrid Multi-Mode Microplate Reader (Winooski, Vermont). DPPH (25 μM) served as 100% radical control, in comparison to other samples. The concentration of remaining DPPH was determined by a standard curve. The free-radical scavenging effect was calculated as previously reported.[36]

We also examined the capability of HA hydrogels as radical scavengers. Hydrogels (100 μL; HA-SH: 4 mg mL^{-1}, F127-SS-DA or F127-DA: 50 mg mL^{-1}) were immersed in 150 μL DPPH solutions (25, 50, and 100 μM). We further checked hydrogels crosslinked by F127-SS-DA or F127-DA of various concentrations (10, 20, and 50 mg mL^{-1}) in 25 μM DPPH solution. These hydrogels with DPPH were kept on a shaker in the dark for 30 min, and the absorbance of the solution was measured using the plate reader at 517 nm. The free radical scavenging effect was calculated. All tests were run in triplicate and averaged.

2.5 Hydrogel swelling and degradation

We evaluated the stability of hydrogels under H_2O_2 conditions. A series of hydrogels (100 μL; HA-SH: 4 mg mL^{-1}, F127-SS-DA or F127-DA: 10, 20, and 50 mg mL^{-1}) were incubated in 1 mL of phosphate buffered saline (PBS) or H_2O_2 solutions (0.5, 10, and 100 mM) at 37 °C on a shaker at 150 rpm. The initial weight of each sample was recorded as W_0. Samples were weighted and recorded at regular time points as W_t. The swelling ratio was defined as W_t/W_0. There were triplicates for each group.

2.6 Cell culture

Human umbilical vein endothelial cells (HUVECs) were obtained from Lonza (Alpharetta, GA). These cells were maintained in VascuLife® VEGF endothelial medium at 37 °C under 5% CO_2, and used before passage 5 in this study.

2.7 Cell viability

Cell viability inside HA hydrogels (40 μL; HA-SH: 4 mg mL^{-1}, F127-SS-DA or F127-DA: 10, 20, and 50 mg mL^{-1}) was examined using a LIVE/DEAD viability kit (L3224, ThermoFisher Scientific, Waltham, MA). Live cells were stained with green fluorescent calcein AM and dead cells with compromised cell membranes were stained with red fluorescent ethidium homodimer-1. The Zeiss LSM 880 laser scanning confocal microscope was used to capture the images of the LIVE/DEAD cell-staining patterns.

AlamarBlue assay (DAL1025, ThermoFisher Scientific, Waltham, MA) was also conducted to characterize cell viability inside the hydrogels according to the manufacture's protocol. Metabolic reduction of alamarBlue was monitored by absorbance measurements at 570 nm and 600 nm using Biotek Synergy H1 Hybrid Multi-Mode Microplate Reader. Metabolic reduction rate was calculated according to the protocol as we reported before.[38]

2.8 Hydrogel-protecting cells against H_2O_2-induced damage

As for cells cultured inside hydrogels, cell density was kept at 1.5 × 10^6/mL hydrogel (40 μL; HA-SH: 4 mg mL^{-1}, F127-SS-DA or F127-DA: 20 mg mL^{-1}). These cells were cultured in a 96-well plate with 150 μL media. Cells cultured on 2D were used as a control. Then the culture media was replaced by H_2O_2-supplemented medium (0, 2.5, 5, and 10 mM) for 1 h. Then alamarBlue and LIVE/DEAD staining as described above were used to evaluate the protection effect of hydrogels on these cells. The DCFDA cellular ROS detection assay kit (Abcam, ab113851) was used to measure intracellular ROS levels with quantification by fluorescence intensity (excitation/emission at 485 nm/535 nm) using Biotek Synergy H1 Hybrid Multi-Mode Microplate Reader.

2.9 Statistical analysis

Data are shown as mean ± S.D. (Standard Deviation). All statistical analyses were performed with Prism 8. Data were analyzed by one-way or two-way ANOVA (analysis of variance) followed by Tukey's post-test where appropriate. The values were considered significantly different at $P < 0.05$.

3 Results

3.1 Synthesis and characterization of F127-SS-DA and F127-DA

We have successfully synthesized F127-DA and F127-SS-DA through Steglich esterification reaction (Fig. 1 and S1†).[39] In particular, acrylate protons on terminal groups of F127-DA backbone provided signals between 5.84 and 6.41 ppm in the ^{1}H NMR spectrum (Fig. 1b). New peak at 4.25 ppm was attributed to the terminal F127 units that close to the reacted acrylate groups. In the ^{1}H NMR spectrum of F127-SS-DA, in comparison with SS-F127-SS (Fig. S1†), new peaks appeared at 4.84 and 5.76 ppm. These proton signals belong to the acrylate groups of the F127-SS-DA backbone (Fig. 1d).

3.2 Antioxidative effect of F127-SS-DA and F127-DA

We next evaluated the antioxidative effect of these synthesized polymers by a radical-scavenging DPPH assay. First, we confirmed that the monomer DTP containing a disulfide group displayed the DPPH scavenging effect in a dose-dependent manner (Fig. S2†). We then examined the antioxidative efficacy of F127-SS-DA and F127-DA. With the increase of its concentrations, F127-SS-DA exhibited an improved radical scavenging effect with an efficiency of 78.3% at 100 mg mL^{-1}

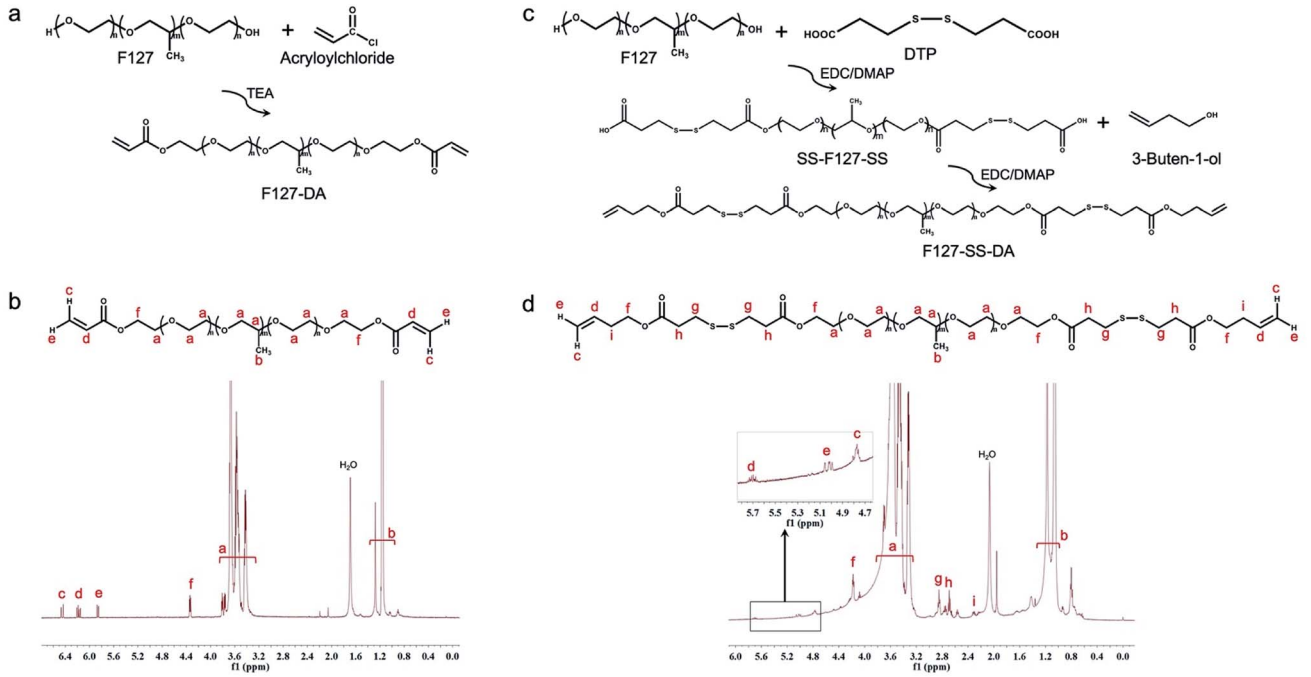

Fig. 1 Synthesis of F127-DA and F127-SS-DA. (a) The synthesis schematic for F127-DA. (b) The structure of F127 confirmed by ^{1}H-NMR. δ 1.1–1.25 (CH_3), 3.4–3.8 ($-CH_2-CH_2-O-$), 4.25 ($COOCH_2$), 5.84–6.41 ($CH_2=CH-$). DA: Di-Acrylate. (c) The synthesis schematic for F127-SS-DA. (d) The structure of F127-SS-DA was confirmed by ^{1}H-NMR. δ 1.1–1.25 (CH_3), 3.4–3.8 ($-CH_2-CH_2-O-$), 2.38 ($C\equiv C-CH_2-$), 2.75 (CH_2COO), 2.95 ($S-CH_2$), 4.25 ($COOCH_2$), 4.84–5.76 ($CH_2=CH-$). DA: di-butenyl ester.

(Fig. 2a). F127-DA, without the disulfide group, did not show apparent scavenging activity independent of its concentrations (0–100 mg mL^{-1}). In particular, at the same concentration of 50 mg mL^{-1}, F127-SS-DA showed significantly higher scavenging efficacy than F127-DA (Fig. 2b; 44.3% *vs.* 6.5%, $P < 0.05$).

3.3 Thermosensitive HA hydrogels

Next we evaluated whether or not the synthesized F127-SS-DA or F127-DA could crosslink HA-SH to form hydrogels. We first mixed the solutions of HA-SH with a series of F127-SS-DA or F127-DA. Since F127 is thermosensitive, we kept these mixtures at 4 °C overnight to avoid the gelation of F127. F127-SS-DA, at the concentrations of 10, 20, and 50 mg mL^{-1}, could crosslink HA-SH to form hydrogels at 4 °C with G' of 29.4, 55.9, and 65.9 Pa, respectively (Fig. 3a). We then examined thermosensitive behaviors of these HA hydrogels by an oscillation temperature sweep test (4–37 °C). All these hydrogels showed temperature-sensitivity with a sharp increase of G' around 20 °C (Fig. 3b). At 37 °C, HA hydrogels with the F127-SS-DA of 10, 20, and 50 mg mL^{-1} exhibited the G' of 190.2, 477.8, and 1892.0 Pa, respectively (Fig. 3c and d). In parallel, F127-DA, at the concentrations of 10, 20, and 50 mg mL^{-1}, could also crosslink HA-SH to form

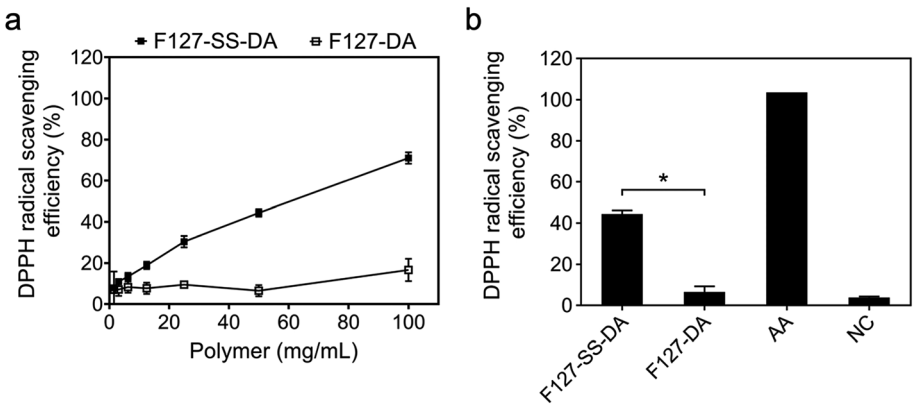

Fig. 2 Antioxidative effects of F127-DA and F127-SS-DA investigated by free radical DPPH assay. (a) F127-SS-DA showed radical scavenging in a dose-dependent manner. F127-DA did not show clear scavenging activity for DPPH (25 μM). (b) DPPH radical scavenging efficiency of polymers of F127-SS-DA and F127-DA at the same concentration of 50 mg mL^{-1}. Ascorbic Acid (AA): 50 mM. Negative Control (NC): 25 μM DPPH without adding polymers. *$P < 0.05$.

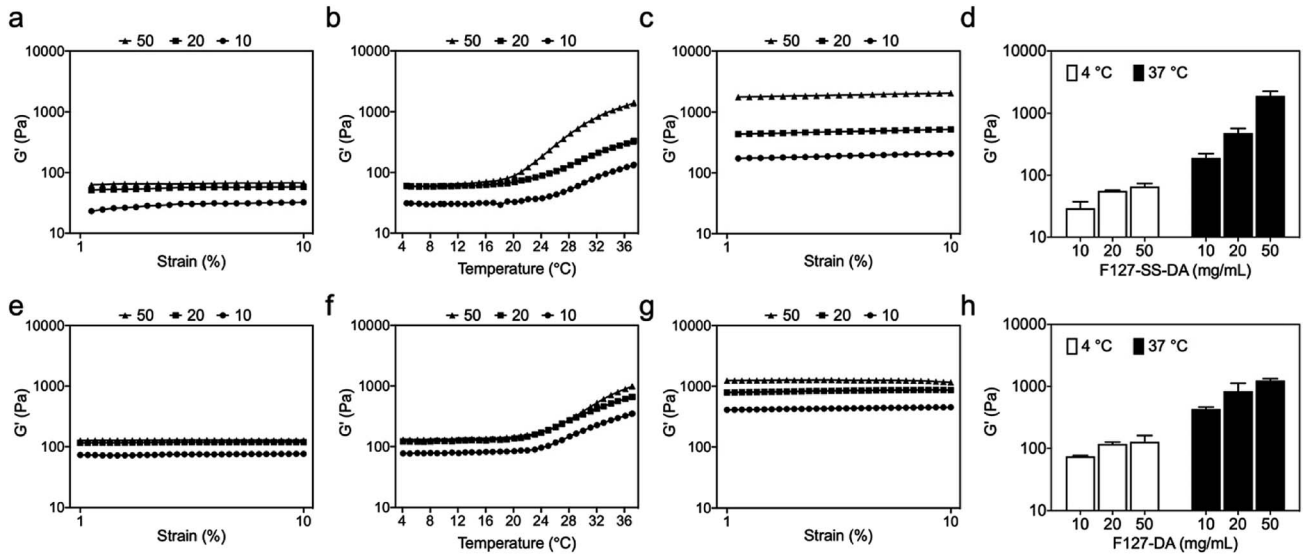

Fig. 3 Rheological characterization of HA hydrogels. (a–d) HA hydrogels with F127-SS-DA of different concentrations of 10, 20, and 50 mg mL. (e–h) HA hydrogels with F127-DA of different concentrations of 10, 20, and 50 mg mL. (a and e) Oscillatory strain sweep of HA hydrogels crosslinked by (a) F127-SS-DA and (e) F127-DA at 4 °C. (b and f) Oscillatory temperature sweep of HA hydrogels crosslinked by (b) F127-SS-DA and (f) F127-DA. (c and g) Oscillatory strain sweep of HA hydrogels crosslinked by (c) F127-SS-DA and (g) F127-DA at 37 °C. (d and h) Shear storage modulus (G') of HA hydrogels crosslinked by (d) F127-SS-DA and (h) F127-DA at 4 °C and 37 °C.

hydrogels at 4 °C with G' of 74.3, 117.9, and 127.6 Pa, respectively (Fig. 3e). Hydrogels with F127-DA showed temperature-sensitivity with a sharp increase of G' around 24 °C (Fig. 3f). At 37 °C, HA hydrogels with the F127-SS-DA of 10, 20, and 50 mg mL^{-1} exhibited the G' of 431.2, 838.6, and 1244.0 Pa, respectively (Fig. 3g and h). In comparison, the increase in G' of F127-SS-DA with temperature is significantly greater than that of F127-DA. The disulfide bond in F127-SS-DA may form the nucleus of a hydrophobic core; around this core the local hydrophobic polypropylene glycol in F127-SS-DA may condense through hydrophobic interactions, which lead to faster gelation and greater increase of G' of the hydrogel with F127-SS-DA (50 mg mL^{-1}) than that with F127-DA (50 mg mL^{-1}). In addition, through the same oscillation sweep test, we examined rat gastrocnemius muscle with a G' around 2.0 kPa (Fig. S3†), which is within the range of our HA hydrogel system. Our hydrogel is injectable, which can easily go through 25 G needle (Fig. S4†).

3.4 Antioxidative effect of HA hydrogels

We further evaluated whether or not HA hydrogels have antioxidative effect through the same DPPH assay above. Under different DPPH concentrations of 25, 50, or 100 μM, when compared to those crosslinked by F127-DA (50 mg mL^{-1}), HA hydrogels with F127-SS-DA (50 mg mL^{-1}) showed significantly higher radical scavenging activities (Fig. 4a; 25 μM: 82.3% *vs.* 20.8%, $P < 0.0001$; 50 μM: 75.1% *vs.* 8.7%, $P < 0.0001$; 100 μM: 46.4% *vs.* 3.5%, $P < 0.0001$). In addition, under 25 μM DPPH, HA hydrogels, with different concentrations of F127-SS-DA of 10, 20, or 50 mg mL^{-1}, exhibited significantly higher radical scavenging activities than those crosslinked by F127-DA at the same concentration (Fig. 4b; 10 mg mL^{-1}: 75.2% *vs.* 27.4%, $P < 0.001$; 20 mg mL^{-1}: 79.1% *vs.* 27.4%, $P < 0.0001$; 50 mg mL^{-1}: 83.0% *vs.* 11.8%, $P < 0.0001$). All these results confirmed the antioxidative capability of HA hydrogels with F127-SS-DA.

3.5 Swelling and degradation of HA hydrogels

We examined the swelling ratios of HA hydrogels crosslinked by F127-SS-DA or F127-DA. HA hydrogels with F127-SS-DA or F127-DA showed the swelling ratios of 118.2% and 106.14% at 2 h, 103.1% and 78.4% at 24 h, 85.9% and 68.1% at 7 days, respectively (Fig. 5a).

Next we checked whether or not these hydrogels respond to H_2O_2. With 10 mM H_2O_2, HA hydrogels crosslinked by F127-SS-DA or F127-DA present the swelling ratios of 120.0% and 108.4% at 2 h, respectively. But HA hydrogel with F127-SS-DA was only stable for 3 days while the hydrogel with F127-DA degraded at day 6. With 100 mM H_2O_2, HA hydrogels crosslinked by F127-SS-DA or F127-DA only last for 1 and 2 day, respectively (Fig. 5a). High concentration of H_2O_2 could oxidize the disulfide group into sulfenic acid group, then sulfinic acid group, and finally stable sulfonic acid group, which may lead to the faster degradation of HA hydrogels with F127-SS-DA.

We further investigated the stability of HA hydrogels at 0.5 mM H_2O_2, which mimics the pathological condition of free radicals inside the ischemic tissue.[40,41] With F127-SS-DA at 10, 20, or 50 mg mL^{-1}, HA hydrogels were stable for 14, 12, and 7 days, respectively. In comparison, HA hydrogels with F127-DA at 10 and 50 mg mL^{-1} were both stable without any response to H_2O_2 (Fig. 5b). Our hydrogels containing disulfide moieties are able to respond to H_2O_2, potentially providing excellent antioxidative effect.

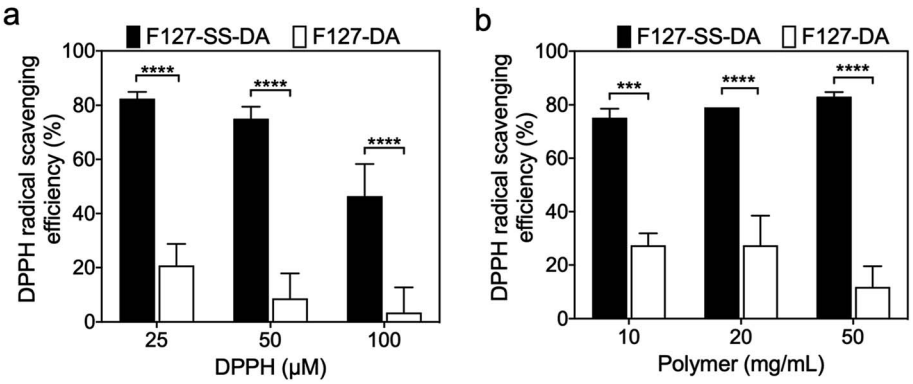

Fig. 4 Antioxidative abilities of HA hydrogels investigated by a DPPH assay. (a) HA hydrogels crosslinked by F127-SS-DA showed significantly higher radical scavenging activities than those crosslinked by F127-DA at the different DPPH concentrations of 25, 50, and 100 μM. HA: 4 mg mL^{-1}. F127-SS-DA or F127-DA: 50 mg mL^{-1}. (b) With different concentrations of 10, 20, and 50 mg mL^{-1}, F127-SS-DA-crosslinked HA hydrogels exhibited significantly higher radical scavenging activities than those crosslinked by F127-DA with the DPPH of 25 μM. ****$P < 0.0001$. ***$0.0001 < P < 0.001$.

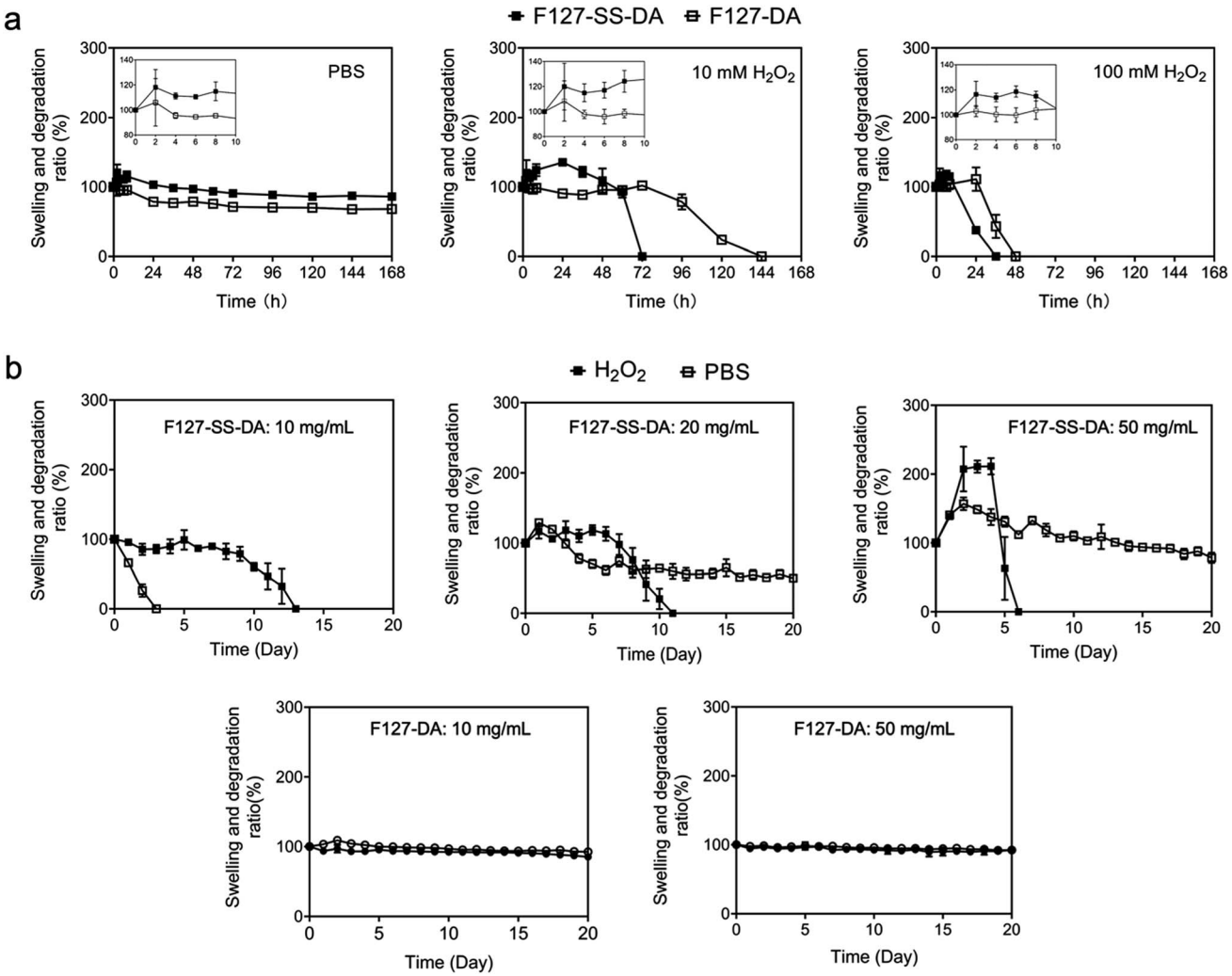

Fig. 5 The swelling and degradation behaviors of HA hydrogels. (a) In phosphate buffer solution (PBS), HA hydrogels crosslinked by F127-SS-DA or F127-DA showed swelling ratios of 103.05% and 78.43% at 24 h, respectively. Under H_2O_2 of 10 or 100 mM, HA hydrogels crosslinked by F127-SS-DA or F127-DA were not stable. HA: 4 mg mL^{-1}. F127-SS-DA or F127-DA: 50 mg mL^{-1}. (b) With F127-SS-DA at 10 mg mL^{-1}, HA hydrogel was only stable for 3 days in PBS. Under H_2O_2 of 0.5 mM, HA hydrogel crosslinked by F127-SS-DA (20 or 50 mg mL^{-1}) showed H_2O_2-responsiive degradation process. HA hydrogels with F127-DA at 10 or 50 mg mL^{-1} is stable without response to H_2O_2 (0.5 mM).

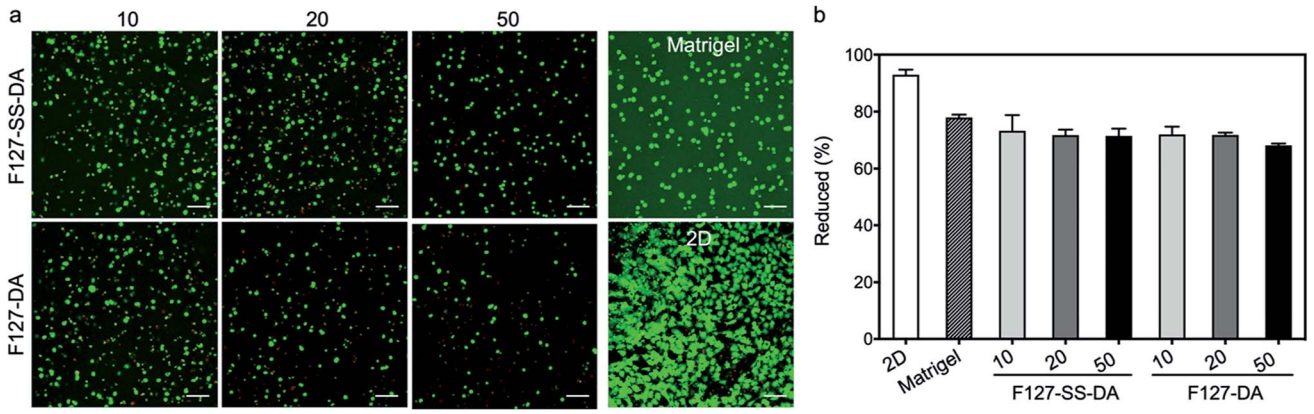

Fig. 6 Cytocompatibility of HA hydrogels. (a) LIVE/DEAD staining of HUVECs inside HA hydrogels crosslinked by F127-SS-DA or F127-DA with different concentrations of 10, 20, and 50 mg mL^{-1}, Matrigel, or under 2D condition. HA: 4 mg mL^{-1}. (b) The viability of HUVECs was investigated by the alamarBlue assay.

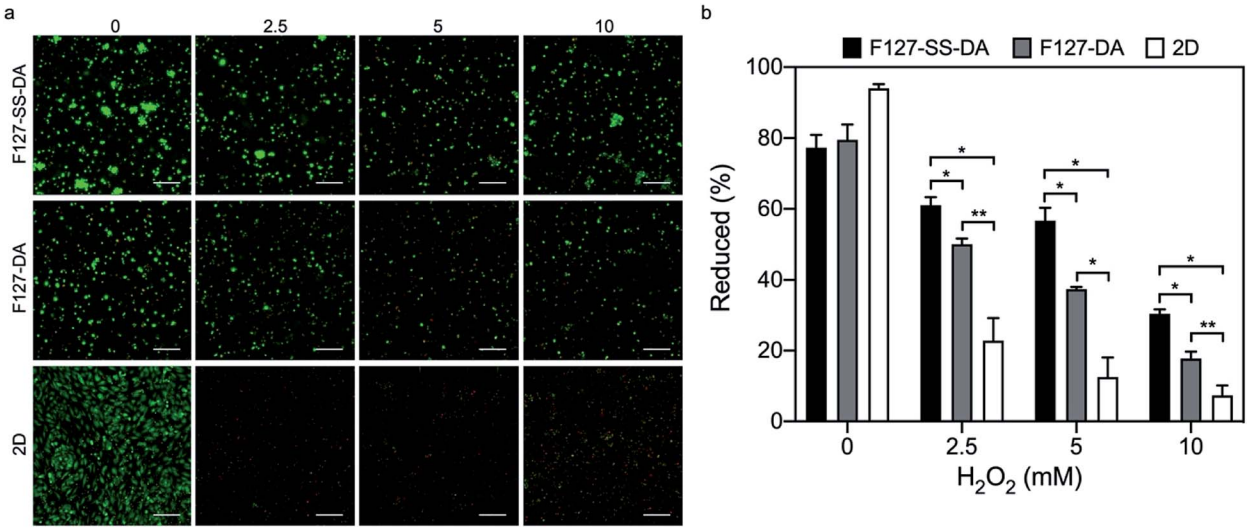

Fig. 7 HA hydrogels protected cells under H_2O_2 condition. (a) LIVE/DEAD staining of HUVECs inside HA hydrogels crosslinked by F127-SS-DA or F127-DA, or under 2D condition with H_2O_2 of 0, 2.5, 5, and 10 mM. HA: 4 mg mL^{-1}. F127-SS-DA or F127-DA: 20 mg mL^{-1}. (b) The viability of HUVECs was investigated by the alamarBlue assay. **$0.001 < P < 0.01$. *$0.01 < P < 0.05$.

3.6 Hydrogel cytocompatibility and cell-protective effect under H_2O_2 condition

We next examined cytocompatibility of HA hydrogels crosslinked by F127-SS-DA or F127-DA. HA hydrogels with F127-SS-DA or F127-DA of 10, 20 or 50 mg mL^{-1}, all showed metabolic reduction about ~70% (Fig. 6; F127-SS-DA: 73.2%, 71.7%, and 71.4%; F127-DA: 71.9%, 71.8%, and 68.1%) at day 2, which is a little bit lower to Matrigel (79.3%). These results demonstrated that our hydrogels have high cytocompatibility.

Since our HA hydrogels exhibited a rapid response to H_2O_2 at high concentration (10 mM, Fig. 5), here we evaluated HUVECs inside HA hydrogels crosslinked by F127-SS-DA or F127-DA, and under 2D condition under H_2O_2 condition (0, 2.5, 5, and 10 mM). Cells under 2D condition showed significantly decreased viabilities and metabolic activities with the increase of H_2O_2 concentrations (Fig. 7; 0: 94.0%, 2.5 mM: 22.8%, 5.0 mM: 12.5%, 10.0 mM: 7.3%). These two HA hydrogels could protect cells compared to those under 2D condition. In particular, cells inside hydrogels with F127-SS-DA, in comparison with those inside hydrogels with F127-DA, displayed significantly higher percentage of metabolic reduction (Fig. 7b; 2.5 mM: 61.1% *vs.* 50.0%, $P < 0.01$; 5.0 mM: 56.7% *vs.* 37.4%, $P < 0.05$; 10.0 mM: 30.4% *vs.* 17.7%, $P < 0.01$). In addition, we investigated the excessive ROS generation in HUVECs with HA hydrogels in response to H_2O_2 (0, 0.5, 1.0, and 2.5 mM). HA hydrogel with F127-SS-DA, compared to that with F127-DA, can significantly reduce intracellular ROS level under H_2O_2 condition (Fig. S6†). All these results confirmed hydrogels with F127-SS-DA can protect cells against H_2O_2-induced damage.

4 Discussion

In this study, we have synthesized a HA-based hydrogel system that meets several important requirements for optimal delivery,

retention, and performance in the mechanically, histologically and biochemically dynamic intramuscular environment of the PAD leg.[42,43] A myopathy is present in the legs of patients with PAD and is central to the functional deterioration seen in this common disease.[21,22,44] This myopathy is produced by low blood flow in the PAD legs and its most important histological characteristics are progressive myofiber degeneration and fibrosis associated with increased oxidative damage.[23–25,45,46] Our data demonstrate that we are able to use disulfide-modified F127 diacrylate to crosslink HA-SH to form a thermosensitive hydrogel with minimal-swelling and with mechanical properties that match those of skeletal muscle. Most importantly, the HA hydrogel with disulfides has shown significant antioxidant capacity, H_2O_2-sensitive degradation, and cell-protective effect against H_2O_2-induced damage, all of which may present unique therapeutic features for the treatment of PAD myopathy.

The latest data on the pathophysiology of PAD suggest that ischemia and ischemia-reperfusion in PAD limbs initiate mitochondrial dysfunction and oxidative damage in the affected limbs, producing injury to every structure in the leg including muscles, nerves, skin, and subcutaneous tissues.[26,47] Accumulating injury in the leg can lead to progressive damage to muscle structure and decline in performance (claudication) and in the more severe stages to loss of the integrity of tissues in the ischemic limb, presenting as tissue loss/gangrene.[26,47] Work from several laboratories including our own has demonstrated that this myopathy is closely related to leg function, daily activity, quality of life, and even mortality of PAD patients.[48–55] Furthermore, worsening of the myopathy is associated with progression of PAD from claudication to rest pain and tissue loss.[23,24,56]

Oxidative stress plays a key role in the development of PAD and its myopathy.[23,47] Tissue-damaging oxidative stress will occur if ROS level is higher than that of cellular antioxidant potential. Several key ROS include H_2O_2, hydroxyl radicals, hypochlorous acid, and superoxide anions. H_2O_2 is not highly reactive itself, but it is an intermediate to both hydroxyl radicals and hypochlorite radical production. Excessive production of these ROS leads to DNA damage, protein modification, lipid peroxidation, disruption of cell signaling, and cellular death. First, we have adopted a free radical (DPPH) scavenging activity assay to evaluate the antioxidative effects of our synthesized polymers F127-SS-DA and F127-DA. F127-SS-DA, with the unique disulfide group, displayed a significantly higher scavenging effect than that of F127-DA (Fig. 2). Furthermore, F127-SS-DA introduces significant antioxidative capacity in the crosslinked HA hydrogel (Fig. 4). Second, H_2O_2 has been widely used to mimic oxidative stress *in vitro*.[36,57] There is an average of $\sim$3 μM H_2O_2 in normal human plasma.[58] Activated macrophages or neutrophils have been shown to release H_2O_2 with a local concentration up to 1000 μM.[40,41] HA hydrogels with F127-SS-DA, exposed to a pathological range (500 μM) of H_2O_2, displayed H_2O_2-responsive degradation (Fig. 5b). More importantly, HUVECs showed significantly decreased viabilities under H_2O_2 over 500 μM (Fig. S5†) while hydrogels with F127-SS-DA could protect cells against H_2O_2-induced damage, even under relative high concentrations of H_2O_2 (Fig. 7b; 2.5–10 mM). Taken together, these results demonstrate the ability of our HA hydrogel to be used as a radical scavenging protective system in the form of a locally delivered antioxidant therapy.

It is worth noting that hydrogels with disulfide moieties have just been explored for other indications. For example, Xu *et al.* have reported a series of injectable HA-based hydrogels crosslinked by hyperbranched poly(β-hydrazide ester) macromers with multi-acrylate end groups with disulfide moieties. These disulfide-containing hydrogels also exhibited H_2O_2-responsive degradation and protected cells under a high ROS environment. However, UV light-induced crosslinking has been required to achieve hydrogels with high stiffness (G' up to kPa).[36,57] Compared with this approach, our hydrogel design relies on temperature change, without requiring an exogenous light source, which may be difficult to achieve *in vivo* following injection. Furthermore, our unique thermosensitive crosslinker significantly reduces the swelling behavior of our HA hydrogel (Fig. 5a; 103.1% at 24 h). The phase transition of F127 inside the hydrogel system (around 20 °C) produces an HA hydrogel with muscle-matching stiffness (Fig. 3; $G' = \sim$2 kPa). In addition, recently Young *et al.* have developed a thermosensitive chitosan-based hydrogel for PAD treatment.[8,59] This injectable hydrogel has shown minimal swelling and high resiliency. Hydrogel gelation is thermally-initiated by ammoniumpersulfate (APS) and *N*,*N*,*N*′,*N*′-tetramethylethylenediamine (TEMED). These required initiators (APS and TEMED) for *in situ* crosslinking need to be kept in low concentrations to avoid their cytotoxicity. As for *in situ* gelation, the rates of initiator consumption and diffusion in the polymer system is also required to be well-controlled, which may be difficult to achieve after injection. Compared with this approach, our hydrogel formation is based on Michael-type addition reaction without requiring any initiators. Our work thus far demonstrates that it is possible to synthesize a hydrogel system that has optimal mechanical, rheological, and biochemical characteristics for intramuscular delivery for the treatment of the ischemic limbs of patients with PAD.

5 Conclusion

In this study, we have developed and optimized a unique HA hydrogel system with antioxidative properties, thermosensitivity, skeletal muscle-matching stiffness, and reduced propensity to swell. We have established that we can use F127-SS-DA with disulfide moieties to enhance the hydrogel with remarkable ROS cytoprotective properties under high H_2O_2 levels. Furthermore, we demonstrated that it is possible to crosslink HA-SH to form a hydrogel with temperature-adjusted stiffness which can be optimized to match that of the skeletal muscle. Finally we have shown that the use of F127 which shrinks under body temperature can significantly reduce the propensity of our hydrogel to swell. Our work indicates that hydrogels have the potential to be optimized for delivery to the mechanically and biochemically dynamic environment of skeletal muscle tissue. Our hydrogel can be used in translational work that evaluates minimally invasive solutions for the

treatment of the myopathy of patients suffering from PAD and other skeletal muscle pathological states.

Author contributions

M. C. and C. L. contributed to the design, execution, and analysis of the described experiments. F. N. contributed to the execution of experiments. X.-Y. L. and I. I. P. contributed to the discussion and analysis of results and preparation of the manuscript. X.-W. L. conceived the project, contributed to design and analysis of the study, and preparation of the manuscript.

Conflicts of interest

The authors declare no competing financial interests.

Acknowledgements

This work was partially supported by funds from University of Nebraska Medical Center, American Heart Association Career Development Award (18CDA34110314), Nebraska Stem Cell Research Project (NE LB606), and R01AG062198. We also acknowledge support by a grant from the National Institute of General Medical Sciences, 1U54GM115458, and the UNMC Center for Heart and Vascular Research. The content is solely the responsibility of the authors and does not necessarily represent the official views of the NIH.

References

1 F. G. R. Fowkes, D. Rudan, I. Rudan, V. Aboyans, J. O. Denenberg, M. M. McDermott, P. E. Norman, U. K. A. Sampson, L. J. Williams, G. A. Mensah and M. H. Criqui, *Lancet*, 2013, **382**, 1329–1340.

2 J. Benjamin Emelia, S. Virani Salim, W. Callaway Clifton, M. Chamberlain Alanna, R. Chang Alexander, S. Cheng, E. Chiuve Stephanie, M. Cushman, N. Delling Francesca, R. Deo, D. de Ferranti Sarah, F. Ferguson Jane, M. Fornage, C. Gillespie, R. Isasi Carmen, C. Jiménez Monik, C. Jordan Lori, E. Judd Suzanne, D. Lackland, H. Lichtman Judith, L. Lisabeth, S. Liu, T. Longenecker Chris, L. Lutsey Pamela, S. Mackey Jason, B. Matchar David, K. Matsushita, E. Mussolino Michael, K. Nasir, M. O'Flaherty, P. Palaniappan Latha, A. Pandey, K. Pandey Dilip, J. Reeves Mathew, D. Ritchey Matthew, J. Rodriguez Carlos, A. Roth Gregory, D. Rosamond Wayne, K. A. Sampson Uchechukwu, M. Satou Gary, H. Shah Svati, L. Spartano Nicole, L. Tirschwell David, W. Tsao Connie, H. Voeks Jenifer, Z. Willey Joshua, T. Wilkins John, H. Y. Wu Jason, M. Alger Heather, S. Wong Sally and P. Muntner, *Circulation*, 2018, **137**, e67–e492.

3 H. Hernandez, S. A. Myers, M. Schieber, D. M. Ha, S. Baker, P. Koutakis, K. S. Kim, C. Mietus, G. P. Casale and I. I. Pipinos, *Ann. Vasc. Surg.*, 2019, **55**, 112–121.

4 Y. Fujita and A. Kawamoto, *Adv. Drug Delivery Rev.*, 2017, **120**, 25–40.

5 S. R. Iyer and B. H. Annex, *JACC: Basic Transl. Sci.*, 2017, **2**, 503–512.

6 Z. Raval and D. W. Losordo, *Circ. Res.*, 2013, **112**, 1288–1302.

7 E. C. Perin, M. P. Murphy, K. L. March, R. Bolli, J. Loughran, P. C. Yang, N. J. Leeper, R. L. Dalman, J. Alexander, T. D. Henry, J. H. Traverse, C. J. Pepine, R. D. Anderson, S. Berceli, J. T. Willerson, R. Muthupillai, A. Gahremanpour, G. Raveendran, O. Velasquez, J. M. Hare, I. Hernandez Schulman, V. S. Kasi, W. R. Hiatt, B. Ambale-Venkatesh, J. A. Lima, D. A. Taylor, M. Resende, A. P. Gee, A. G. Durett, J. Bloom, S. Richman, P. G'Sell, S. Williams, F. Khan, E. Gyang Ross, M. R. Santoso, J. Goldman, D. Leach, E. Handberg, B. Cheong, N. Piece, D. DiFede, B. Bruhn-Ding, E. Caldwell, J. Bettencourt, D. Lai, L. Piller, L. Simpson, M. Cohen, S. L. Sayre, R. W. Vojvodic, L. Moye, R. F. Ebert, R. D. Simari and A. T. Hirsch, *Circulation*, 2017, **135**, 1417–1428.

8 S. A. Young, S. E. Sherman, T. T. Cooper, C. Brown, F. Anjum, D. A. Hess, L. E. Flynn and B. G. Amsden, *Biomaterials*, 2018, **159**, 146–160.

9 A. A. Foster, R. E. Dewi, L. Cai, L. Hou, Z. Strassberg, C. A. Alcazar, S. C. Heilshorn and N. F. Huang, *Biomater. Sci.*, 2018, **6**, 614–622.

10 J. L. Ungerleider, T. D. Johnson, M. J. Hernandez, D. I. Elhag, R. L. Braden, M. Dzieciatkowska, K. G. Osborn, K. C. Hansen, E. Mahmud and K. L. Christman, *JACC: Basic Transl. Sci.*, 2016, **1**, 32–44.

11 J. L. Ungerleider and K. L. Christman, *Stem Cells Transl. Med.*, 2014, **3**, 1090–1099.

12 J. A. DeQuach, J. E. Lin, C. Cam, D. Hu, M. A. Salvatore, F. Sheikh and K. L. Christman, *Eur. Cells Mater.*, 2012, **23**, 400–412.

13 N. Rao, G. Agmon, M. T. Tierney, J. L. Ungerleider, R. L. Braden, A. Sacco and K. L. Christman, *ACS Nano*, 2017, **11**, 3851–3859.

14 K. L. Christman, *Science*, 2019, **363**, 340–341.

15 P. Simon, M. T. Kasimir, G. Seebacher, G. Weigel, R. Ullrich, U. Salzer-Muhar, E. Rieder and E. Wolner, *Eur. J. Cardiothorac. Surg.*, 2003, **23**, 1002–1006, discussion 1006.

16 E. M. Anderson, E. A. Silva, Y. Hao, K. D. Martinick, S. A. Vermillion, A. G. Stafford, E. G. Doherty, L. Wang, E. J. Doherty, P. M. Grossman and D. J. Mooney, *J. Vasc. Res.*, 2017, **54**, 288–298.

17 J. P. Gong, Y. Katsuyama, T. Kurokawa and Y. Osada, *Adv. Mater.*, 2003, **15**, 1155–1158.

18 C. B. Rodell, N. N. Dusaj, C. B. Highley and J. A. Burdick, *Adv. Mater.*, 2016, **28**, 8419–8424.

19 K. J. Henderson, T. C. Zhou, K. J. Otim and K. R. Shull, *Macromolecules*, 2010, **43**, 6193–6201.

20 M. K. Jaiswal, J. R. Xavier, J. K. Carrow, P. Desai, D. Alge and A. K. Gaharwar, *ACS Nano*, 2016, **10**, 246–256.

21 I. I. Pipinos, A. R. Judge, J. T. Selsby, Z. Zhu, S. A. Swanson, A. A. Nella and S. L. Dodd, *Vasc. Endovascular Surg.*, 2007, **41**, 481–489.

22 I. I. Pipinos, A. R. Judge, J. T. Selsby, Z. Zhu, S. A. Swanson, A. A. Nella and S. L. Dodd, *Vasc. Endovascular Surg.*, 2008, **42**, 101–112.

23 P. Koutakis, D. J. Weiss, D. Miserlis, V. K. Shostrom, E. Papoutsi, D. M. Ha, L. A. Carpenter, R. D. McComb, G. P. Casale and I. I. Pipinos, *Redox Biol.*, 2014, **2**, 921–928.
24 D. J. Weiss, G. P. Casale, P. Koutakis, A. A. Nella, S. A. Swanson, Z. Zhu, D. Miserlis, J. M. Johanning and I. I. Pipinos, *J. Transl. Med.*, 2013, **11**, 230.
25 I. I. Pipinos, A. R. Judge, Z. Zhu, J. T. Selsby, S. A. Swanson, J. M. Johanning, B. T. Baxter, T. G. Lynch and S. L. Dodd, *Free Radicals Biol. Med.*, 2006, **41**, 262–269.
26 P. Koutakis, A. Ismaeel, P. Farmer, S. Purcell, R. S. Smith, J. L. Eidson and W. T. Bohannon, *Physiol. Rep.*, 2018, **6**, e13650.
27 X. Li, X. Liu, N. Zhang and X. Wen, *J. Neurotrauma*, 2014, **31**, 1431–1438.
28 X. Li, S. Y. Tzeng, X. Liu, M. Tammia, Y.-H. Cheng, A. Rolfe, D. Sun, N. Zhang, J. J. Green, X. Wen and H.-Q. Mao, *Biomaterials*, 2016, **84**, 157–166.
29 X. Li, C. Zhang, A. E. Haggerty, J. Yan, M. Lan, M. Seu, M. Yang, M. M. Marlow, I. Maldonado-Lasunción, B. Cho, Z. Zhou, L. Chen, R. Martin, Y. Nitobe, K. Yamane, H. You, S. Reddy, D.-P. Quan, M. Oudega and H.-Q. Mao, *Biomaterials*, 2020, **245**, 119978.
30 X. Li, B. Cho, R. Martin, M. Seu, C. Zhang, Z. Zhou, J. S. Choi, X. Jiang, L. Chen, G. Walia, J. Yan, M. Callanan, H. Liu, K. Colbert, J. Morrissette-McAlmon, W. Grayson, S. Reddy, J. M. Sacks and H.-Q. Mao, *Sci. Transl. Med.*, 2019, **11**, eaau6210.
31 X. Li, X. Liu, L. Cui, C. Brunson, W. Zhao, N. R. Bhat, N. Zhang and X. Wen, *FASEB J.*, 2013, **27**, 1127–1136.
32 M. Slevin, S. Kumar and J. Gaffney, *J. Biol. Chem.*, 2002, **277**, 41046–41059.
33 J. Zhang, A. Skardal and G. D. Prestwich, *Biomaterials*, 2008, **29**, 4521–4531.
34 Y.-n. Sun, G.-r. Gao, G.-l. Du, Y.-j. Cheng and J. Fu, *ACS Macro Lett.*, 2014, **3**, 496–500.
35 Z. Li, F. Zhou, Z. Li, S. Lin, L. Chen, L. Liu and Y. Chen, *ACS Appl. Mater. Interfaces*, 2018, **10**, 25194–25202.
36 Q. Xu, M. Venet, W. Wang, J. Creagh-Flynn, X. Wang, X. Li, Y. Gao, D. Zhou, M. Zeng, I. Lara-Sáez, A. Sigen, H. Tai and W. Wang, *ACS Appl. Mater. Interfaces*, 2018, **10**, 39494–39504.
37 Q. Xu, C. He, C. Xiao and X. Chen, *Macromol. Biosci.*, 2016, **16**, 635–646.
38 X. Li, X. Liu, W. Zhao, X. Wen and N. Zhang, *Acta Biomater.*, 2012, **8**, 2087–2095.
39 B. Neises and W. Steglich, *Angew. Chem., Int. Ed. Engl.*, 1978, **17**, 522–524.
40 P. A. Hyslop, Z. Zhang, D. V. Pearson and L. A. Phebus, *Brain Res.*, 1995, **671**, 181–186.
41 J. R. Burgoyne, S.-i. Oka, N. Ale-Agha and P. Eaton, *Antioxid. Redox Signaling*, 2013, **18**, 1042–1052.
42 R. A. Becker, K. Cluff, N. Duraisamy, G. P. Casale and I. I. Pipinos, *J. Surg. Res.*, 2017, **220**, 79–87.
43 M. N. Schieber, R. M. Hasenkamp, I. I. Pipinos, J. M. Johanning, N. Stergiou, H. K. DeSpiegelaere, J. H. Chien and S. A. Myers, *J. Vasc. Surg.*, 2017, **66**, 178–186, e112.
44 K. I. Makris, A. A. Nella, Z. Zhu, S. A. Swanson, G. P. Casale, T. L. Gutti, A. R. Judge and I. I. Pipinos, *Vascular*, 2007, **15**, 336–343.
45 P. Koutakis, D. Miserlis, S. A. Myers, J. K. Kim, Z. Zhu, E. Papoutsi, S. A. Swanson, G. Haynatzki, D. M. Ha, L. A. Carpenter, R. D. McComb, J. M. Johanning, G. P. Casale and I. I. Pipinos, *J. Histochem. Cytochem.*, 2015, **63**, 256–269.
46 I. I. Pipinos, S. A. Swanson, Z. Zhu, A. A. Nella, D. J. Weiss, T. L. Gutti, R. D. McComb, B. T. Baxter, T. G. Lynch and G. P. Casale, *Am. J. Physiol.: Regul., Integr. Comp. Physiol.*, 2008, **295**, R290–R296.
47 S. S. Signorelli, S. Scuto, E. Marino, A. Xourafa and A. Gaudio, *Antioxidants*, 2019, **8**, 367.
48 M. M. McDermott, K. Liu, L. Tian, J. M. Guralnik, M. H. Criqui, Y. Liao and L. Ferrucci, *J. Am. Coll. Cardiol.*, 2012, **59**, 1159–1167.
49 P. K. Garg, K. Liu, L. Ferrucci, J. M. Guralnik, M. H. Criqui, L. Tian, R. Sufit, T. Nishida, H. Tao, Y. Liao and M. M. McDermott, *J. Am. Geriatr. Soc.*, 2011, **59**, 1855–1863.
50 N. S. Evans, K. Liu, M. H. Criqui, L. Ferrucci, J. M. Guralnik, L. Tian, Y. Liao and M. M. McDermott, *Vasc. Med.*, 2011, **16**, 3–11.
51 M. M. McDermott, L. Ferrucci, J. Guralnik, L. Tian, K. Liu, F. Hoff, Y. Liao and M. H. Criqui, *Circulation*, 2009, **120**, 1048–1055.
52 J. R. Thompson, S. A. Swanson, G. Haynatzki, P. Koutakis, J. M. Johanning, P. R. Reppert, E. Papoutsi, D. Miserlis, Z. Zhu, G. P. Casale and I. I. Pipinos, *Ann. Surg.*, 2015, **261**, 605–610.
53 A. W. Gardner, D. E. Parker, P. S. Montgomery, S. M. Blevins, A. M. Teague and A. I. Casanegra, *Angiology*, 2014, **65**, 491–496.
54 E. P. Brass, W. R. Hiatt and S. Green, *Vasc. Med.*, 2004, **9**, 293–301.
55 J. D. Anderson, F. H. Epstein, C. H. Meyer, K. D. Hagspiel, H. Wang, S. S. Berr, N. L. Harthun, A. Weltman, J. M. Dimaria, A. M. West and C. M. Kramer, *J. Am. Coll. Cardiol.*, 2009, **54**, 628–635.
56 D. M. Ha, L. C. Carpenter, P. Koutakis, S. A. Swanson, Z. Zhu, M. Hanna, H. K. DeSpiegelaere, I. I. Pipinos and G. P. Casale, *J. Transl. Med.*, 2016, **14**, 39.
57 W. Wang, J. Chen, M. Li, H. Jia, X. Han, J. Zhang, Y. Zou, B. Tan, W. Liang, Y. Shang, Q. Xu, A. Sigen, W. Wang, J. Mao, X. Gao, G. Fan and W. Liu, *ACS Appl. Mater. Interfaces*, 2019, **11**, 2880–2890.
58 F. Lacy, M. T. Kailasam, D. T. O'Connor, G. W. Schmid-Schönbein and R. J. Parmer, *Hypertension*, 2000, **36**, 878–884.
59 J. Dhillon, S. A. Young, S. E. Sherman, G. I. Bell, B. G. Amsden, D. A. Hess and L. E. Flynn, *J. Biomed. Mater. Res., Part A*, 2019, **107**, 571–585.

